

Journal of Materials Chemistry A

Accepted Manuscript



This is an *Accepted Manuscript*, which has been through the Royal Society of Chemistry peer review process and has been accepted for publication.

Accepted Manuscripts are published online shortly after acceptance, before technical editing, formatting and proof reading. Using this free service, authors can make their results available to the community, in citable form, before we publish the edited article. We will replace this *Accepted Manuscript* with the edited and formatted *Advance Article* as soon as it is available.

You can find more information about *Accepted Manuscripts* in the [Information for Authors](#).

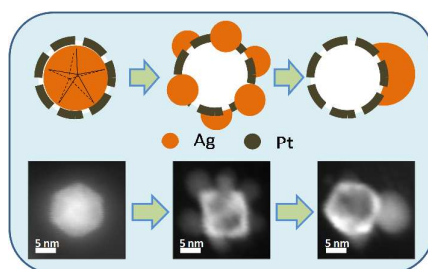
Please note that technical editing may introduce minor changes to the text and/or graphics, which may alter content. The journal's standard [Terms & Conditions](#) and the [Ethical guidelines](#) still apply. In no event shall the Royal Society of Chemistry be held responsible for any errors or omissions in this *Accepted Manuscript* or any consequences arising from the use of any information it contains.

Graphic abstract

Bimetallic Ag-hollow Pt heterodimers *via* inside-out migration of Ag in core-shell Ag-Pt nanoparticles at elevated temperature

Hui Liu^{ab} and Jun Yang^{a*}

Bimetallic Ag-hollow Pt heterodimers was fabricated *via* the inside-out migration of Ag in core-shell Ag-Pt nanoparticles at elevated temperature.



Cite this: DOI: 10.1039/c0xx00000x

www.rsc.org/xxxxxx

ARTICLE TYPE

Bimetallic Ag-hollow Pt heterodimers *via* inside-out migration of Ag in core-shell Ag-Pt nanoparticles at elevated temperature†

Hui Liu^{ab} and Jun Yang^{a*}

Received (in XXX, XXX) Xth XXXXXXXXX 20XX, Accepted Xth XXXXXXXXX 20XX

DOI: 10.1039/b000000x

Bimetallic heterodimers often exhibit unique and superior properties different from the each one of the constituent materials due to the synergistic effect between the two component metals. Herein, we present the synthesis of bimetallic heterodimers consisting of Ag and hollow structured Pt nanoparticles (Ag-hPt) through a structural transformation at elevated temperature. In this strategy, core-shell Ag-Pt nanoparticles are first prepared, and subsequently converted into bimetallic Ag-hPt heterodimers via the inside-out migration of Ag in core-shell Ag-Pt nanoparticles. The heating treatment at elevated temperature is employed to promote the inside-out diffusion of Ag from the core region of the core-shell nanoparticles. The resulting bimetallic Ag-hPt heterodimers display significantly different optical and catalytic properties from their core-shell Ag-Pt nanoparticle precursors. The synthetic technique and mechanistic understanding may provide new opportunities to design and fabricate heterogeneous nanostructures with interesting physicochemical properties.

1 Introduction

Bimetallic heterodimers, in which one metal is distributed at single site on the surface of another metal particles, might exhibit unique and superior properties different from the each one of the constituent materials due to the synergistic effect between the two component metals. For example, the Pt nanoparticles modified by Au clusters were found to display excellent stability for the electrocatalysis of oxygen reduction reaction (ORR) at room temperature due to the electronic interaction between Au and Pt in the heterodimers.¹ A number of strategies including localized overgrowth,² high temperature reduction,³ plasmon-mediated synthesis,⁴ manipulation of reaction kinetics,⁵ and selective transformation⁶ have been developed for the synthesis of bimetallic heterodimers. Recently, Puentes and coworkers reported the fabrication of Au-Pt heterodimers at room temperature using oleylamine as reducing agent, and found that the Pt seeds play an important role for the nucleation and growth of Au region in the heterodimer structures.⁷ However, in comparison with the abundant studies on the semiconductor/metal oxide-noble metal heterodimers,^{8,9} the literatures reported on heterodimers consisting of two chemically distinct metals are still very limited due to the lack of synthetic inaccessibility. The most commonly used seed-mediated growth method usually results in the formation of bimetallic nanoparticles with core-shell or dendritic aggregates.^{10,11} Considering the further exploration of the properties and consequent applications of these heterogeneous nanostructures, the development of effective approaches for the production of bimetallic heterodimers would be undoubtedly important and pose significant challenges.

In the present work, we present a facile and high-yield

approach to the synthesis of bimetallic heterodimers consisting of Ag and hollow structured Pt nanoparticles, labeled as Ag-hollow Pt (Ag-hPt), which is based on an unique diffusion phenomenon of Ag in core-shell Ag-Pt nanoparticles with Ag residing in the core region. In this strategy, core-shell Ag-Pt nanoparticles are first prepared as starting templates dispersed in an organic medium. The core-shell Ag-Pt templates are subsequently converted into Ag-hPt heterodimers via the inside-out migration of Ag in core-shell Ag-Pt nanoparticles. The heating treatment at elevated temperature is employed to promote the inside-out diffusion of Ag from the core region of the core-shell nanoparticles. The purpose of this study is to provide an unique strategy (inside-out migration of Ag in core-shell Ag-Pt nanoparticles) to fabricate bimetallic Ag-hollow Pt nanoparticles with heterodimeric structures and to demonstrate the physical/chemical properties of a bimetallic system might be tuned by tailoring its structure (by relegating Ag to the core or on the shell region in bimetallic Ag-Pt nanoparticles). As we will see, the resulting bimetallic Ag-hPt heterodimers and their core-shell Ag-Pt nanoparticle precursors are significantly different in optical and catalytic properties. It should be noted that in this work we are not seeking an electrocatalysts with enhanced activity. The oxygen reduction reaction (ORR) was only chosen as a typical example to demonstrate the effect of the different structure on the catalytic property of a bimetallic system. This study offers a vivid example to demonstrate the tuning of the material properties by means of a structural tailoring. In addition, the mechanistic understanding of the structural transformation from core-shell to heterogeneous nanoparticles might be used to design and fabricate other heteronanostructures for a given application.

2 Experimental

2.1 General materials

Potassium tetrachloroplatinate(II) (K_2PtCl_4 , 98%), silver nitrate ($AgNO_3$, 99%), aqueous $HClO_4$ solution (70%, ACS reagent), and Nafion 117 solution (5% in a mixture of lower aliphatic alcohols and water) from Aladdin Reagents, oleylamine (70%, technical grade) from Sigma-Aldrich, methanol (99%) and toluene (99.5%) from Beijing Chemical Works, and Vulcan XC-72 carbon powders (XC-72C, BET surface area = $250\text{ m}^2/\text{g}$ and average particle size = 40–50 nm) from Cabot Corporation, were used as received. All glassware and Teflon-coated magnetic stir bars were cleaned with *aqua regia*, followed by copious washing with de-ionized water before drying in an oven.

2.2 Synthesis of core-shell Ag-Pt nanoparticles

An one-pot approach was used for the synthesis of Ag-Pt nanoparticles with core-shell structures. In brief, 68 mg of $AgNO_3$ (0.4 mmol) and 83 mg of K_2PtCl_4 (0.2 mmol) were added to 20 ml of oleylamine in a three-necked flask equipped with a condenser and a stir bar. The solution was brought to and kept at 165°C for 2 h under flowing N_2 for the reduction of Ag^+ and Pt^{2+} by oleylamine. The Ag and Pt precursor molar ratio was controlled at 2/1. After reaction, the core-shell Ag-Pt nanoparticles were purified by precipitation with methanol, centrifugation, washing with methanol, and re-dispersed in 20 mL of toluene.

2.3 Synthesis of bimetallic Ag-hPt heterodimers

The bimetallic Ag-hPt heterodimers were converted from the core-shell Ag-Pt nanoparticles. To accelerate the conversion from core-shell Ag-Pt nanoparticles to bimetallic Ag-hPt heterodimers, 10 mL of core-shell Ag-Pt particle solution in toluene was placed in a three-necked flask equipped with a condenser and a stir bar, which was then aged at 80°C for 72 h under air and constant stirring.

2.4 Particle characterizations

Transmission electron microscopy (TEM), high resolution TEM (HRTEM), and scanning TEM (STEM) were performed on the JEOL JEM-2100 and FEI Tecnai G² F20 electron microscope operating at 200 kV with a supplied software for automated electron tomography. For the TEM measurements, a drop of the nanoparticle solution was dispensed onto a 3-mm carbon-coated copper grid. Excessive solution was removed by an absorbent paper, and the sample was dried under vacuum at room temperature. An energy dispersive X-ray spectroscopy (EDX) analyzer attached to the TEM operating in the scanning transmission electron microscopy (STEM) mode was used to analyze the chemical compositions of the synthesized nanoparticles. UV-visible spectra of the organic suspensions of core-shell Ag-Pt nanoparticles and bimetallic Ag-hPt heterodimers were collected on a Hitachi U-3900 spectrophotometer. Powder X-ray diffraction (XRD) patterns were recorded on a Rigaku D/Max-3B diffractometer, using $Cu\ K\alpha$ radiation ($\lambda = 1.54056\text{ \AA}$). X-ray photoelectron spectroscopy (XPS) was conducted on a VG ESCALAB MKII spectrometer. Samples for XRD and XPS analyses were concentrated from the

toluene solution of nanoparticles to 0.5 mL using flowing N_2 . 10 mL of methanol was then added to precipitate the nanoparticles, which were recovered by centrifugation, washed with methanol several times, and then dried at room temperature in vacuum.

2.5 Electrochemical measurements

Electrochemical measurements were carried out in a standard three-electrode cell connected to a Bio-logic VMP3 (with EC-lab software version 9.56) potentiostat. A leak-free Ag/AgCl (saturated with KCl) electrode was used as the reference electrode. The counter electrode was a platinum mesh ($1\times 1\text{ cm}^2$) attached to a platinum wire.

For the loading of the catalyst on Vulcan XC-72 carbon support, a calculated amount of carbon powder (78 mg) was added to 10 mL of toluene solution of core-shell Ag-Pt nanoparticles or bimetallic Ag-hPt heterodimers. After stirring the mixture for 24 h, the nanoparticles/C were collected by centrifugation, washed twice with methanol, and then dried at room temperature in vacuum. Upon the high loading efficiency of the nanoparticles on XC-72C carbon powders from the toluene (~99%),^{8k} 20 wt% Pt on carbon support was achieved.

The working electrode was a thin layer of Nafion-impregnated catalyst cast on a vitreous carbon disk. This electrode was prepared by ultrasonically dispersing 10 mg of the nanoparticles/C in 10 mL of aqueous solution containing 4 mL of ethanol and 0.1 mL of Nafion. A calculated volume of the ink was dispensed onto the 5 mm glassy carbon disk electrode to produce a nominal catalyst loading of $20\ \mu\text{g cm}^{-2}$ (Pt basis). The carbon electrode was then dried in a stream of warm air at 70°C for 1 h.

The room temperature cyclic voltammograms of core-shell Ag-Pt nanoparticles and bimetallic Ag-hPt heterodimers in argon-purged $HClO_4$ (0.1 M) were recorded between -0.2 V and 1 V at 50 mV s^{-1} and used for the determination of electrochemically active surface area (ECSA) of Pt. The catalyst performance in room-temperature oxygen reduction reaction (ORR) was evaluated in $HClO_4$ electrolyte solution (0.1 M) using a glass carbon rotating disk electrode (RDE) at a rotation speed of 1600 rpm. Negative-going linear sweep voltammograms were recorded from 0.8 V to 0 V at 20 mV s^{-1} at room temperature in the presence of bubbling ultra-pure oxygen to maintain a saturated oxygen atmosphere near the working electrode. In the ORR polarization curve, the current density was normalized in reference to the ECSA to obtain the specific activities.

3 Results and discussion

In the strategy developed in this work, the preparation of core-shell Ag-Pt nanoparticles is an important step preceding the fabrication of bimetallic Ag-hPt heterodimers. The core-shell Ag-Pt nanoparticles were synthesized using a co-reduction of $AgNO_3$ and K_2PtCl_4 in oleylamine at elevated temperature. Although both Ag(I) and Pt(II) cation precursors were heated in one-pot, the Ag(I) precursor was preferentially reduced because the reduction of Ag-oleylamine complexes was kinetically more facile. The fast kinetics resulted in the formation of multiply twinned Ag nanoparticles which seeded the subsequent deposition of Pt. The as-prepared colloidal solution was then cooled down to room temperature, and the nanoparticles were

precipitated, washed with methanol, and redispersed into toluene.

3.1 Core-shell Ag-Pt nanoparticles

The typical TEM and STEM images of the core-shell Ag-Pt nanoparticles were shown in Fig. 1a and b. The nanoparticles were nearly monodispersed, with an average diameter of approximately 12.9 nm. The EDX analysis (Fig. 1c) of an arbitrary single particle boxed in the high-angle annular dark-field STEM image (Fig. 1b) confirmed that the particle was indeed composed of Ag and Pt. The formation of core-shell structure could be demonstrated by the elemental profiles of arbitrarily chosen single particles in the high-angle annular dark-field STEM mode. As indicated in Fig. 1d, the Pt signal was present throughout the particle whereas the Ag signal was detected only in the core region (approximately 9 nm). The core-shell Ag-Pt nanoparticles were predominately multiply twinned with an icosahedral morphology, as illustrated by the HRTEM images sampled from isolated particles (Fig. 1e, f, and g), which showed the particles in different orientations (along a 2-fold symmetry axis in Fig. 1e, along a 3-fold symmetry axis in Fig. 1f, and along a 5-fold symmetry axis in Fig. 1g).¹²

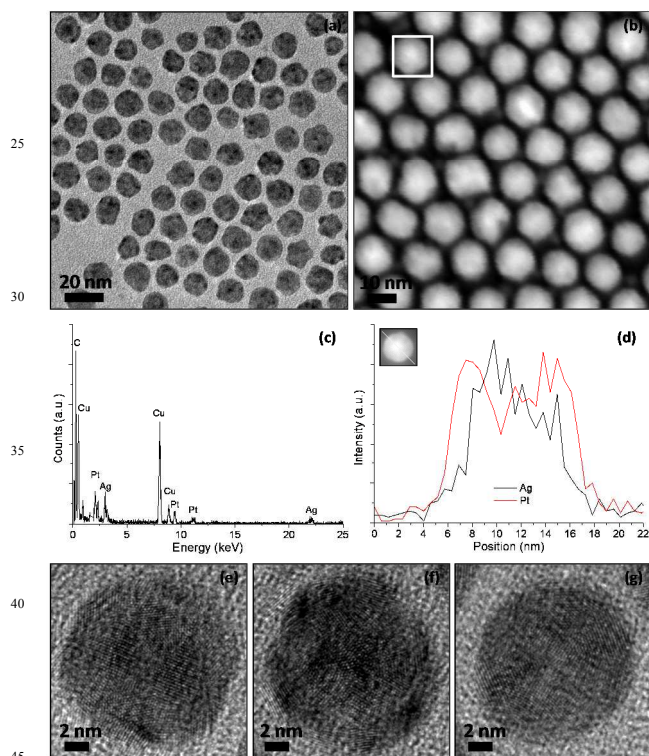


Fig. 1 (a) TEM image, (b) STEM image, (c) STEM-EDX spectrum, (d) elemental profiles, and (e,f,g) HRTEM images of icosahedral core-shell Ag-Pt nanoparticles synthesized in oleylamine by a one-pot approach.

3.2 Bimetallic Ag-hPt heterodimers

After heating the core-shell Ag-Pt colloidal solution in toluene at 80°C for 72 h under air, Ag was migrated to the surface of Pt shells from the interior of core-shell Ag-Pt nanoparticles, resulting in the formation of bimetallic heterodimers consisting of Ag and Pt nanoparticles with a hollow interior. The TEM and STEM images (Fig. 2a and b) after heating treatment in toluene

showed that only heterodimers with strong imaging contrast in different domains were observed in the final products, which were clearly distinct from the starting core-shell nanoparticles (Fig. 1a and b). The void space between the core and the outer shell regions in the Pt domains, formed upon the inside-out migration of the Ag cores by heating treatment, was discernible by the strong brightness contrast in TEM and STEM images, while Ag appeared as lighter domains having solid-state interfaces with the Pt sections. As indicated by Fig. 2c, the EDX analysis of an arbitrary single dimer boxed in the high-angle annular dark-field STEM image (Fig. 2b) confirmed the presence of Ag and Pt after heating treatment of core-shell Ag-Pt nanoparticles. A more direct evidence for the formation of Ag-hPt heterodimers was provided by the line scanning analysis of an arbitrary single dimer in the high-angle annular dark-field STEM mode. As shown in Fig. 2d, the Pt signal was present at one side throughout the heterodimer whereas the Ag signal was detected only at the other side. The interplanar spacings of approximately 0.24 nm and 0.23 nm indicated in the HRTEM images of the bimetallic Ag-hPt heterodimers (Fig. 2e and f) correspond to the (111) planes of face-centered cubic (fcc) Ag and Pt, respectively. A comparison of TEM and STEM images of bimetallic Ag-hPt heterodimers (Fig. 2a and b) and core-shell Ag-Pt nanoparticles (Fig. 1a and b) showed virtually no change in the particle size and morphology for the remaining Pt domains, suggesting that the inside-out migration of Ag cores from core-shell Ag-Pt nanoparticles did not cause the collapse of the particle geometry.

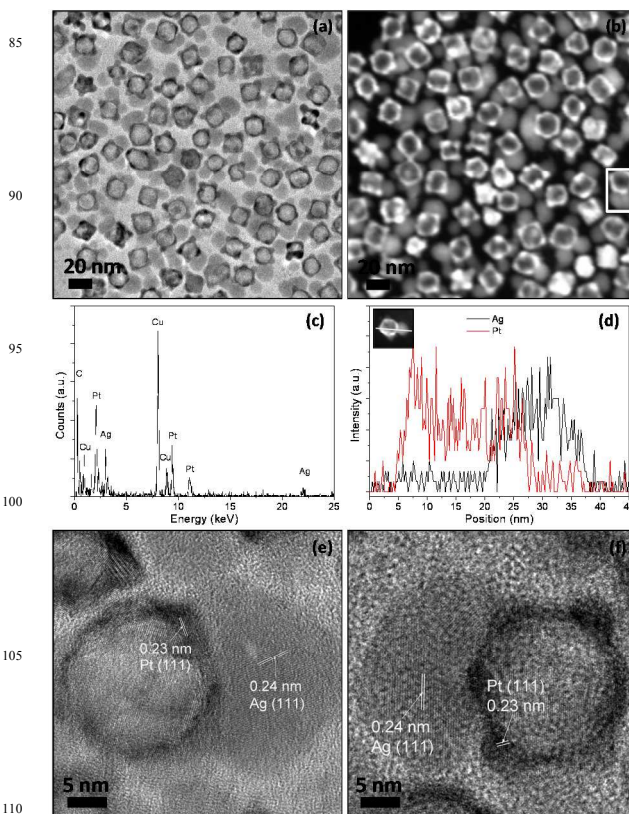


Fig. 2 (a) TEM image, (b) STEM image, (c) STEM-EDX spectrum, (d) elemental profiles, and (e,f) HRTEM images of bimetallic Ag-hPt heterodimers synthesized *via* the inside-out migration of Ag in core-shell Ag-Pt nanoparticles at elevated temperature.

3.3 Mechanism for the fabrication of bimetallic Ag-hPt heterodimers from core-shell Ag-Pt nanoparticles

The fabrication of bimetallic Ag-hPt heterodimers *via* the inside-out migration of Ag in core-shell Ag-Pt nanoparticles can be rationalized by the scheme shown in Fig. 3. The twinned Ag seeds were inherently unstable and could slowly be etched by dissolved O_2 and Cl^- dissociated from the Pt precursor to generate $Ag(I)$ ions.^{13,14} These $Ag(I)$ ions were then diffused out through the discontinuous Pt shells, which were produced during the epitaxial deposition of Pt atoms on the Ag seeds with a large number of imperfections on their surfaces, due to the $Ag(I)$ concentration gradient between the interior of core-shell Ag-Pt nanoparticles and the surrounding solution. At suitable temperature (e.g. 80°C), the $Ag(I)$ ions diffused out from core-shell Ag-Pt nanoparticles were re-reduced by excess oleylamine in the solution to form single crystalline Ag nanoparticles decorated on the outer surface of the Pt shell.¹³ The Ag nanoparticles grew with the continued outward diffusion of $Ag(I)$ ions until the Ag core was completely depleted, leaving behind a colloidal solution of bimetallic Ag-hPt with heterogeneous nanostructures. Finally, the Ag nanoparticles on the surface of the Pt shell underwent a ripening process, e.g. Ostwald ripening or electrochemical ripening,^{15,16} to form larger and more stable domains on the surface of Pt shell. The evolution of Ag nanoparticles on the surface of hollow Pt domains might be supported by the two STEM images of core-shell Ag-Pt system obtained at early stages of heating treatment (40 h and 60 h after heating treatment at elevated temperature under air), as shown in Fig. S1 of Electronic Supplementary Information (ESI), which illustrated that at early stage the Ag nanoparticles were formed at multiple sites on the surface of hollow Pt domains. However, the ripening observed in TEM might not exactly represent the case in solution, since the electron beam might have affected the process.¹⁷

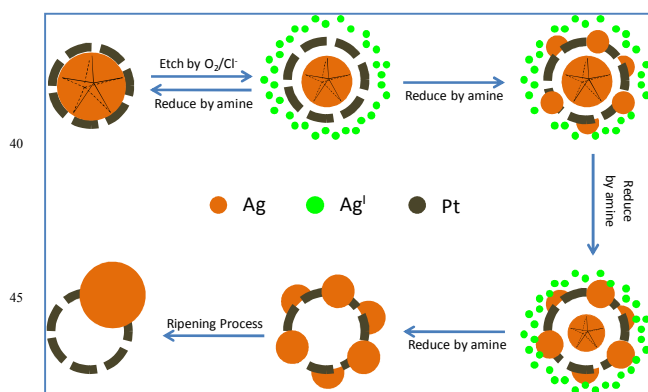


Fig. 3 A schematic illustration showing the formation of bimetallic Ag-hPt heterodimers *via* the inside-out migration of Ag in core-shell Ag-Pt nanoparticles.

3.4 Optical properties of core-shell Ag-Pt nanoparticles and bimetallic Ag-hPt heterodimers

Fig. 4 showed the absorption spectra recorded from organic suspensions of the as-synthesized core-shell Ag-Pt nanoparticles and Ag-hPt heterodimers. For comparison, in Fig. 4 the

absorption spectrum of the monometallic Ag nanoparticles prepared by oleylamine reduction of $AgNO_3$ in the absence of K_2PtCl_4 was also shown, which gave surface plasmon resonance (SPR) peak at 392 nm. For the core-shell Ag-Pt nanoparticles, the SPR peak associated with Ag cores was observed at 377 nm, clearly indicating that the SPR for Ag is blue-shifted as a result of coating with a Pt shell. This phenomenon can be attributed to the decrease in surface electron density in the Ag core, which is driven by electron donation from Ag to Pt because of the higher electronegativity of Pt (2.28) relative to Ag (1.83). However, for the bimetallic Ag-hPt heterodimers prepared *via* inside-out migration of Ag in core-shell particles, the SPR peak associated with the Ag domains in the heterodimers appeared at longer wavelengths (400 nm). In principle, the optical properties of metal nanoparticles were determined by the interaction of the incoming light with the free conduction electrons. The plasmon resonance condition was fulfilled and absorption would occur when there was a coupling between the frequency of the alternating electric field of the electromagnetic radiation and the oscillation of conduction electrons. Since this was a surface effect, the asymmetric incorporation of another metal nanoparticles could change the resonance condition of the latter, as observed for the bimetallic Ag-hPt heterodimers. These results demonstrated that the optical properties of Ag nanoparticles could be affected by their nanostructures formed with a second metal.

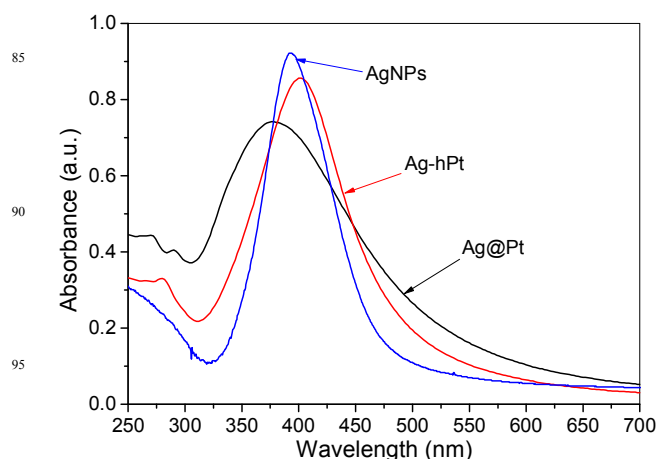


Fig. 4 UV-Visible spectra recorded from organic suspensions of the core-shell Ag-Pt nanoparticles (black line), bimetallic Ag-hPt heterodimers (red line), and the monometallic Ag nanoparticles prepared by oleylamine reduction of $AgNO_3$ at elevated temperature in the absence of K_2PtCl_4 (blue line).

3.5 Electrochemical activity of core-shell Ag-Pt nanoparticles and bimetallic Ag-hPt heterodimers

To demonstrate the effect of the structure of the bimetallic Ag-Pt systems on the catalytic properties, the core-shell Ag-Pt nanoparticles and bimetallic Ag-hPt heterodimers were loaded on Vulcan carbon and examined for their electrocatalytic activities towards the room-temperature oxygen reduction reaction (ORR). Cyclic voltammograms of core-shell Ag-Pt/C and bimetallic Ag-hPt/C in argon-purged 0.1 M $HClO_4$ at room temperature were used to obtain the electrochemical active surface areas (ECSAs)

from the hydrogen adsorption/desorption regions (-0.2–0.1 V vs Ag/AgCl). As shown in Fig. 5a, the ECSAs normalized by the mass of Pt for core-shell Ag-Pt nanoparticles and bimetallic Ag-hPt heterodimers were $40.6 \text{ m}^2 \text{ g}_{\text{Pt}}^{-1}$ and $48.8 \text{ m}^2 \text{ g}_{\text{Pt}}^{-1}$, respectively. The inside-out migration of Ag from core-shell Ag-Pt nanoparticles may lead to the increase of ECSAs by releasing the inner surface of Pt shell, whereas the growth of Ag domains on the outer surface of Pt shell would result in the decrease of ECSAs due to the coherent interfaces between hollow Pt and Ag in the heterodimers, which may induce some blockage of the surface area of the Pt shells. These two effects might have offset each other, such that the ECSA of bimetallic Ag-hPt heterodimers

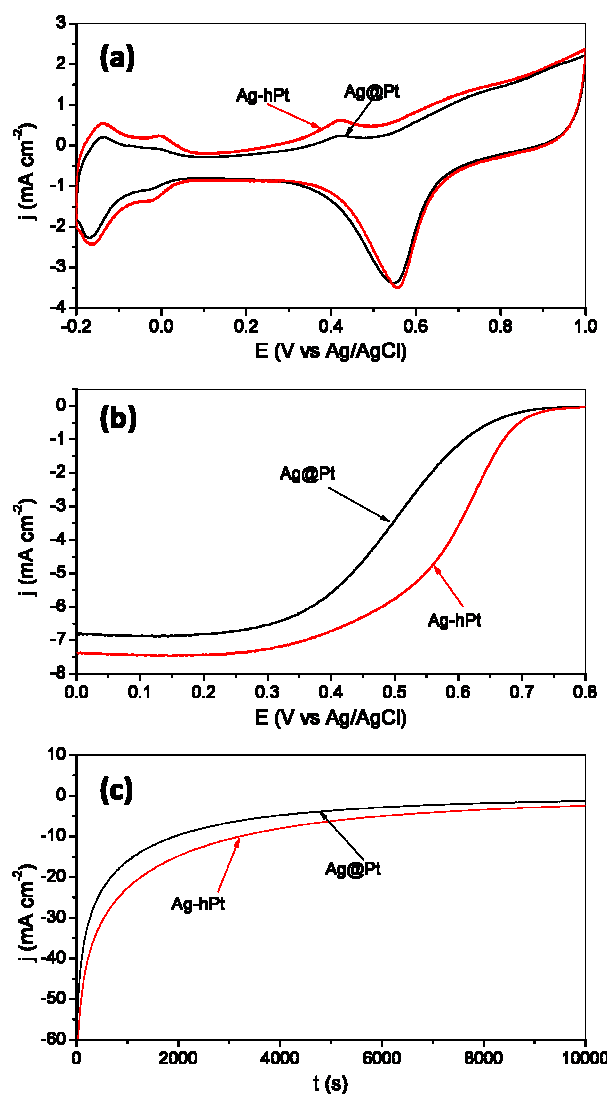


Fig. 5 (a) Cyclic voltammograms of core-shell Ag-Pt nanoparticles and bimetallic Ag-hPt heterodimers in argon-purged HClO_4 (0.1 M) at room temperature, scan rate: 50 mV s^{-1} ; (b) ORR polarization curves for core-shell Ag-Pt nanoparticles and bimetallic Ag-hPt heterodimers, recorded at room temperature in an O_2 -saturated HClO_4 solution (0.1 M) at a sweep rate of 20 mV s^{-1} and a rotating speed of 1600 rpm; (c) chronoamperograms of core-shell Ag-Pt nanoparticles and bimetallic Ag-hPt heterodimers at 0.6 V in an O_2 -saturated HClO_4 solution (0.1 M) at room temperature and a rotating speed of 1600 rpm.

was only slightly higher than that of core-shell Ag-Pt nanoparticles. In cyclic voltammograms (Fig. 5a), the slight increase in ECSA may account for the small positive shift of the peak related to reduction of oxygen containing adsorbed species for bimetallic Ag-hPt heterodimers in comparison with that for core-shell Ag-Pt nanoparticles.

Fig. 5b showed the ORR polarization curves in the potential range of 0.8 to 0 V for core-shell Ag-Pt nanoparticles and bimetallic Ag-hPt heterodimers in oxygen-saturated 0.1 M HClO_4 at room temperature. The half-wave potentials for the core-shell Ag-Pt nanoparticles and bimetallic Ag-hPt heterodimers were 518 mV and 606 mV, respectively. It has been noted that the half-wave potential for bimetallic Ag-hPt heterodimers was much more positive than that of core-shell Ag-Pt nanoparticles, indicating that the Pt shells in the Ag-hPt heterodimers have higher catalytic activity for ORR in comparison with that of core-shell Ag-Pt nanoparticles under the experimental conditions. Furthermore, chronoamperometry of core-shell Ag-Pt nanoparticles and bimetallic Ag-hPt heterodimers at 0.6 V in oxygen-saturated 0.1 M HClO_4 solution was used to obtain some indications of the long-term performance of the catalysts in ORR. As shown in Fig. 5c, the "steady-state" specific activity of bimetallic Ag-hPt heterodimers was higher than that of core-shell Ag-Pt nanoparticles after 2.5 h, indicating the greater stability of the bimetallic heterodimers.

Considering the electronic coupling between Ag and Pt were present both in core-shell Ag-Pt nanoparticles and bimetallic Ag-hPt heterodimers although it was asymmetric in the latter, the lower catalytic activity of the core-shell Ag-Pt nanoparticles in comparison with that of the bimetallic Ag-hPt heterodimers could be attributed to the tensile effect imposed on the Pt shell by the Ag core in core-shell structures. Since Ag has larger lattice parameter (0.4090 nm) than that of Pt (0.3923 nm), the Ag cores would exert a tensile effect on the Pt atoms deposited on their surfaces.^{10f} The XRD patterns in ESI Fig. S2 was used to indicate the crystalline nature of the core-shell Ag-Pt nanoparticles and bimetallic Ag-hPt heterodimers. Since Ag has similar crystalline structure and lattice parameters as those of Pt, the XRD patterns in Fig. S2 could be a convolution of the XRD features of these crystallographically similar metals. In addition, as indicated, compared to the core-shell Ag-Pt nanoparticles, a small negative shift in 2θ ($\sim 0.2^\circ$) was observed for the XRD peaks of Ag-hPt heterodimers, which was induced by the elimination of the tensile effect due to the inside-out migration of Ag cores from core-shell Ag-Pt particles. The tensile effect of Ag core on Pt shell in core-shell Ag-Pt nanoparticles was also observed experimentally in the Pt-4f XPS spectra. When the tensile strain occurs, the width of the d-band and the energy of its center change as the overlap changes, although the degree of d-band filling remains the same. The atoms are pushed away and the average coordination number decreases, leading to the decreased overlap of the d orbitals, and consequently the band narrows.¹⁸ The center of the d-band moves up in order to maintain the same filling degree. Further close to the Fermi level, the d-electrons have become less stable, resulting in the decrease of Pt XPS binding energies, which are related to the ionization of these metal atoms.¹⁹ As shown in ESI Fig. S3, the 4f XPS spectra of Pt in core-shell Ag-Pt nanoparticles and bimetallic Ag-hPt heterodimers were analyzed. The Pt 4f spectra

can be deconvoluted into two pairs of doublets. The more intense doublet (at 70.2 eV and 73.5 eV for core-shell Ag-Pt, 70.5 eV and 73.8 eV for bimetallic Ag-hPt heterodimers) corresponded to Pt(0), while the second and weaker doublet, with binding energies of approximate 1.4 eV higher than those of Pt(0), could be assigned to Pt(II) as in PtO and Pt(OH)₂.²⁰ As expected, in comparison with those in bimetallic Ag-hPt heterodimers, an appreciable shift to lower values was observed for Pt 4f_{7/2} and 4f_{5/2} binding energies in the core-shell Ag-Pt nanoparticles.

It is generally accepted that the common ORR process, i.e. the series 4 electron pathway, must involve both the breaking of an O–O bond and the formation of O–H bonds.²¹ The most active Pt-based catalyst should have the d-band center with an intermediate value since the optimal ORR catalyst needs to facilitate both bond-breaking and bond-making steps without hindering one or the other.²² For core-shell Ag-Pt nanoparticles, the tensile effect of Ag core on Pt shell, which leads to narrower d-band, results in an up-shift of the d-band center of the Pt shell. As has been demonstrated,²³ the surface of a Pt-based catalyst with high value of d-band center tends to bind adsorbents too strongly, thereby enhancing the kinetics of dissociation reactions producing these adsorbents. In this case, the Pt shells may suffer from hindered bond-making step, therefore are less active for ORR. On the other hand, the bimetallic Ag-hPt heterodimers showed good catalytic activity toward ORR possibly because they have a more suitable d-band center to balance the breaking of O-O bonds and the formation of O-H bonds.

4 Conclusions

In summary, bimetallic heterodimers consisting of Ag and hollow structured Pt nanoparticles were fabricated through the heating treatment of core-shell Ag-Pt nanoparticles. This strategy was based on an unique diffusion phenomenon of Ag in core-shell Ag-Pt nanoparticles with Ag residing in the core region. Core-shell Ag-Pt nanoparticles were first prepared, which were subsequently converted into Ag-hPt heterodimers via the inside-out migration of Ag in core-shell Ag-Pt nanoparticles. The heating treatment at elevated temperature was employed to promote the inside-out diffusion of Ag from the core region of the core-shell nanoparticles. The resulting bimetallic Ag-hPt heterodimers and their core-shell Ag-Pt nanoparticle precursors displayed significant difference in optical and catalytic properties. This study offers a vivid example to demonstrate the tuning of the material properties by means of a structural tailoring. The technique may be extended to explore the heterodimers composed of nobles other than Ag and Pt. This could result in some interesting examples with technological importance.

Acknowledgement

Financial support from the 100 Talents Program of the Chinese Academy of Sciences, National Natural Science Foundation of China (No.: 21173226, 21376247), and State Key Laboratory of Multiphase Complex Systems, Institute of Process Engineering, Chinese Academy of Sciences (MPCS-2012-A-11, MPCS-2011-D-08, MPCS-2010-C-02) is gratefully acknowledged.

Notes and references

- ⁵⁵ ^a State Key Laboratory of Multiphase Complex Systems, Institute of Process Engineering, Chinese Academy of Sciences, Beijing, China 100190. Fax: 86-10-8254 4915; Tel: 86-10-8254 4915; E-mail: jyang@mail.ipe.ac.cn
- ^b University of Chinese Academy of Sciences, No. 19A Yuquan Road, Beijing, China 100049
- †Electronic Supplementary Information (ESI) available: STEM images to show the evolution of Ag domains on the surface of Pt shells, and XPS spectra of Pt 4f to show the tensile effect of Ag on Pt in core-shell Ag-Pt nanoparticles. See DOI:10.1039/b000000x/
- 1 J. Zhang, K. Sasaki and R. R. Adzic, *Science*, 2007, **315**, 220.
 - 2 a) H. Lee, S. E. Habas, G. A. Somorjai and P. Yang, *J. Am. Chem. Soc.*, 2008, **130**, 5406; b) B. Lim, H. Kobayashi, T. Yu, J. Wang, M. J. Kim, Z.-Y. Li, M. Rycenga and Y. Xia, *J. Am. Chem. Soc.*, 2010, **132**, 2506.
 - 3 a) T. Pellegrino, A. Fiore, E. Carlino, C. Giannini, P. D. Cozzoli, G. Ciccarella, M. Respaud, L. Palmirotti, R. Cingolani and L. Manna, *J. Am. Chem. Soc.*, 2006, **128**, 6690; b) J.-S. Choi, H. J. Choi, D. C. Jung, J.-H. Lee and J. Cheon, *Chem. Commun.*, 2008, 2197; c) C. Wang, W. Tian, Y. Ding, Y.-Q. Ma, Z. L. Wang, N. M. Marković, V. R. Stamenkovic, H. Daimon and S. Sun, *J. Am. Chem. Soc.*, 2010, **132**, 6524.
 - 4 M. R. Langille, J. Zhang and C. A. Mirkin, *Angew. Chem., Int. Ed.*, 2011, **50**, 3543.
 - 5 J. Zeng, C. Zhu, J. Tao, M. Jin, H. Zhang, Z.-Y. Li, Y. Zhu and Y. Xia, *Angew. Chem. Int. Ed.*, 2012, **51**, 2354.
 - 6 L. Bai, Y. Kuang, J. Luo, D. G. Evans and X. Sun, *Chem. Commun.*, 2012, **48**, 6963.
 - 7 S. I. Lim, M. Varon, I. Ojea-Jiménez, J. Arbiol and V. Puntès, *J. Mater. Chem.*, 2011, **21**, 11518.
 - 8 a) T. Mokari, E. Rothenberg, I. Popov, R. Costi and U. Banin, *Science*, 2004, **304**, 1787; b) W. L. Shi, H. Zeng, Y. Sahoo, T. Y. Ohulchanskyy, Y. Ding, Z. L. Wang, M. Swihart and P. N. Prasad, *Nano Lett.*, 2006, **6**, 875; c) J. Yang, L. Levina, E. H. Sargent and S. O. Kelley, *J. Mater. Chem.*, 2006, **16**, 4025; d) S. E. Habas, P. D. Yang and T. Mokari, *J. Am. Chem. Soc.*, 2008, **130**, 3294; e) J. Yang and J. Y. Ying, *Chem. Commun.*, 2009, 3187; f) J. Yang, E. H. Sargent, S. O. Kelley and J. Y. Ying, *Nature Mater.*, 2009, **8**, 683; g) N. Zhao, L. Li, T. Huang and L. Qi, *Nanoscale*, 2010, **2**, 2418; h) R. Costi, A. E. Saunders and U. Banin, *Angew. Chem. Int. Ed.*, 2010, **49**, 4878; i) L. Carbone and P. D. Cozzoli, *Nano Today*, 2010, **5**, 449; j) E. Shaviv, O. Schubert, M. Alves-Santos, G. Goldoni, R. D. Felice, F. Vallée, N. D. Fatti, U. Banin and C. Sönnichsen, *ACS Nano*, 2011, **5**, 4712; k) J. Yang and J. Y. Ying, *Angew. Chem. Int. Ed.*, 2011, **50**, 4637; l) S. Chakraborty, G. Xing, Y. Xu, S. W. Ngiam, N. Mishra, T. C. Sum and Y. Chan, *Small*, 2011, **7**, 2847; m) W. Hu, H. Liu, F. Ye, Y. Ding and J. Yang, *CrystEngComm*, 2012, **14**, 7049; n) X. Ding, Y. Zou and J. Jiang, *J. Mater. Chem.*, 2012, **22**, 23169; o) N. E. Motl, J. F. Bondi and R. E. Schaak, *Chem. Mater.*, 2012, **24**, 1552; p) X. Ma, Y. Zhao, X. Jiang, W. Liu, S. Liu and Z. Tang, *ChemPhysChem*, 2012, **13**, 2531; q) H. Liu, F. Ye, H. Cao, G. Ji, J. Y. Lee and J. Yang, *Nanoscale*, 2013, **5**, 6901; r) D. Wang, X. Li, H. Li, L. Li, X. Hong, Q. Peng and Y. Li, *J. Mater. Chem. A*, 2013, **1**, 1587; s) X. Ding, Y. Zou, F. Ye, J. Yang and J. Jiang, *J. Mater. Chem. A*, 2013, **1**, 11880.
 - 9 a) H. Yu, M. Chen, P. M. Rice, S. X. Wang, R. L. White and S. Sun, *Nano Lett.*, 2005, **5**, 379; b) H. Gu, Z. Yang, J. Gao, C. K. Chang and B. Xu, *J. Am. Chem. Soc.*, 2005, **127**, 34; c) Y. Li, Q. Zhang, A. V. Nurmikko and S. Sun, *Nano Lett.*, 2005, **5**, 1689; d) A. Figuerola, A. Fiore, R. D. Corato, A. Falqui, C. Giannini, E. Micotti, A. Lascialfari, M. Corti, R. Cingolani, T. Pellegrino, P. D. Cozzoli and L. Manna, *J. Am. Chem. Soc.*, 2008, **130**, 1477; e) J. Jiang, H. Gu, H. Shao, E. Devlin, G. C. Papaefthymiou and J. Y. Ying, *Adv. Mater.*, 2008, **20**, 4403; f) C. Xu, J. Xie, D. Ho, C. Wang, N. Kohler, E. G. Walsh, J. R. Morgan, Y. E. Chin and S. Sun, *Angew. Chem. Int. Ed.*, 2008, **47**, 173; g) C. Xu, B. Wang and S. Sun, *J. Am. Chem. Soc.*, 2009, **131**, 4216; h) C. Wang, H. Daimon and S. Sun, *Nano Lett.*, 2009, **9**, 1493; i) Y. Lee, M. A. Garcia, N. A. F. Huls and S. Sun, *Angew. Chem. Int. Ed.*, 2010, **49**, 1271; j) C. Wang, H. Yin, S. Dai and S. Sun, *Chem. Mater.*, 2010, **22**, 3277; k) J. Huang, Y. Sun, S. Huang, K. Yu, Q. Zhao, F. Peng, H. Yu, H. Wang, J. Yang, J.

Mater. Chem., 2011, **21**, 17930; l) J. S. Beveridge, M. R. Buck, J. F. Bondi, R. Misra, P. Schiffer, R. E. Schaak and E. Williams, *Angew. Chem. Int. Ed.*, 2011, **50**, 9875; m) M. R. Buck, J. F. Bondi and R. E. Schaak, *Nature Chem.*, 2012, **4**, 37.

- 10 a) J. Yang, J. Y. Lee, L. X. Chen and H.-P. Too, *J. Phys. Chem. B*, 2005, **109**, 5468; b) S. E. Habas, H. Lee, V. Radmilovic, G. A. Somorjai and P. Yang, *Nature Mater.*, 2007, **6**, 692; c) J. Luo, L. Wang, D. Mott, P. N. Njoki, Y. Lin, T. He, Z. Xu, B. N. Wanjala, I. S. Lim and C. Zhong, *Adv. Mater.*, 2008, **20**, 4342; d) W.-P. Zhou, X. Yang, M. B. Vukmirovic, B. E. Koel, J. Jiao, G. Peng, M. Mavrikakis and R. R. Adzic, *J. Am. Chem. Soc.*, 2009, **131**, 12755; e) J. Yang, X. Chen, X. Yang and J. Y. Ying, *Energy Environ. Sci.*, 2012, **5**, 8976; f) J. Yang, J. Yang and J. Y. Ying, *ACS Nano*, 2012, **6**, 9373.
- 15 11 a) L.-F. Zhang, S.-L. Zhong and A.-W. Xu, *Angew. Chem. Int. Ed.*, 2013, **52**, 645; b) S. Zhou, K. McIlwrath, G. Jackson and B. Eichhorn, *J. Am. Chem. Soc.*, 2006, **128**, 1780; c) Z. Peng and H. Yang, *Nano Res.*, 2009, **2**, 406; d) F. Wang, C. Li, L.-D. Sun, H. Wu, T. Ming, J. Wang, J. C. Yu and C.-H. Yan, *J. Am. Chem. Soc.*, 2011, **133**, 1106; e) B. Lim, M. Jiang, P. H. C. Camargo, E. C. Cho, J. Tao, X. Lu, Y. Zhu and Y. Xia, *Science*, 2009, **324**, 1302; f) Z. Peng and H. Yang, *J. Am. Chem. Soc.*, 2009, **131**, 7542; g) S. Guo, S. Dong and E. Wang, *ACS Nano*, 2010, **4**, 547.
- 20 12 a) J. Reyes-Gasca, S. Tehuacanero-Núñez, J. M. Montejano-Carrzales, X. Gao and M. Jose-Yacaman, *Top. Catal.*, 2007, **46**, 23; b) Q. Zhang, J. Xie, J. Yang and J. Y. Lee, *ACS Nano*, 2009, **3**, 139; c) T. Ling, L. Xie, J. Zhu, H. Yu, H. Ye, R. Yu, Z. Cheng, L. Liu, L. Liu, G. Yang, Z. Cheng, Y. Wang and X. Ma, *Nano Lett.*, 2009, **9**, 1572.
- 30 13 B. Wiley, T. Herricks, Y. Sun and Y. Xia, *Nano Lett.*, 2004, **4**, 1733.
- 14 H. Liu, J. Qu, Y. Chen, J. Li, F. Ye, J. Y. Lee and J. Yang, *J. Am. Chem. Soc.*, 2012, **134**, 11602.
- 15 W. Ostwald, *Z. Phys. Chem.*, 1897, **22**, 289.
- 16 T. Mokari, C. G. Sztrum, A. Salant, E. Rabani and U. Banin, *Nature Mater.*, 2005, **14**, 855.
- 35 17 J. Yang and J. Y. Ying, *J. Am. Chem. Soc.*, 2010, **132**, 2114.
- 18 L. A. Kibler, A. M. El-Aziz, R. Hoyer and D. M. Kolb, *Angew. Chem. Int. Ed.*, 2005, **44**, 2080.
- 40 19 a) S. Kumar and S. Zou, *Langmuir*, 2007, **23**, 7365; b) K. Lee, O. Savadogo, A. Ishihara, S. Mitsushima, N. Kamiya and K. Ota, *J. Electrochem. Soc.*, 2006, **153**, A20.
- 20 a) J. Yang, J. Y. Lee, T. C. Deivaraj and H.-P. Too, *Langmuir*, 2003, **19**, 10361; b) J. Yang, T. C. Deivaraj, H.-P. Too and J. Y. Lee, *J. Phys. Chem. B*, 2004, **108**, 2181.
- 45 21 a) N. M. Marković and P. N. Ross, *Surf. Sci. Rep.*, 2002, **45**, 117; b) V. R. Stamenkovic, B. S. Mun, M. Arenz, K. J. J. Mayrhofer, C. A. Lucas, G. F. Wang, P. N. Ross and N. M. Marković, *Nature Mater.*, 2007, **6**, 241; c) V. R. Stamenkovic, B. Fowler, B. S. Mun, G. F. Wang, P. N. Ross, C. A. Lucas and N. M. Marković, *Science*, 2007, **315**, 493.
- 50 22 a) J. Zhang, M. B. Vukmirovic, K. Sasaki, A. U. Nilekar, M. Mavrikakis and R. R. Adzic, *J. Am. Chem. Soc.*, 2005, **127**, 12480; b) J. Zhang, M. B. Vukmirovic, Y. Xu, M. Mavrikakis and R. R. Adzic, *Angew. Chem. Int. Ed.*, 2005, **44**, 2132.
- 55 23 Y. Xu, A. V. Ruba and M. Mavrikakis, *J. Am. Chem. Soc.*, 2004, **126**, 4717.

Graphical abstract

Bimetallic Ag-hollow Pt heterodimers via inside-out migration of Ag in core-shell Ag-Pt nanoparticles at elevated temperature

Hui Liu^{ab} and Jun Yang^{a*}

80 Bimetallic Ag-hollow Pt heterodimers was fabricated via the inside-out migration of Ag in core-shell Ag-Pt nanoparticles at elevated temperature.

